Formation and Desorption of Oxygen Species in Nanoporous Crystal $12CaO{\cdot}7Al_2O_3$

Shuwu Yang,[†] Junko N. Kondo,[‡] Katsuro Hayashi,[†] Masahiro Hirano,[†] Kazunari Domen,*[,‡] and Hideo Hosono*[,†,§]

Transparent Electro-Active Materials Project, ERATO, Japan Science and Technology Corporation, KSP C-1232, 3-2-1 Sakado, Tatatsu-ku, Kawasaki 213-0012, Japan, Chemical Resources Laboratory and Materials and Structures Laboratory, Tokyo Institute of Technology, 4259 Nagatsuta, Midori-ku, Yokohama 226-8503, Japan

Received August 15, 2003. Revised Manuscript Received October 23, 2003

The formation and desorption mechanisms of oxygen species in nanoporous crystal $12CaO{\cdot}7Al_2O_3$ ($C_{12}A_7$) are studied by temperature-programmed desorption (TPD), electron-spin resonance (ESR), and Raman spectroscopy. Various oxygen ion species, including O^-, O_2^-, and O_2^{2-}, are observed to exist in $C_{12}A_7$ at high concentrations ($\sim 10^{20}$ cm^{-3}). The desorption of these oxygen species in $C_{12}A_7$ is proposed to proceed in three steps: (1) diffusion of oxygen species from bulk to the surface (rate-limiting step), (2) decomposition of oxygen species into oxygen molecules, and (3) release of molecular oxygen into the gas phase. Oxygen species in $C_{12}A_7$ can be regenerated by heating in an O_2 atmosphere at higher than 400 °C, and the concentrations of O^- and O_2^- increase with temperature. More O_2^- is formed than O^- at low activation temperatures, whereas nearly equal amounts of O^- and O_2^- are formed at high temperatures around 1350 °C. At 400−700 °C, a considerable amount of molecular oxygen, O_2, is suggested to be present together with other oxygen species. The formation of oxygen ion species occurs in a manner reverse to the desorption processes, with the first step involving diffusion of oxygen from the atmosphere into nanocages of $C_{12}A_7$.

1. Introduction

The compound $12CaO{\cdot}7Al_2O_3$ ($C_{12}A_7$), one of the crystalline phases in the system of CaO and Al_2O_3,[1−3] is a constituent in aluminous cements. It was first synthesized by Rankin and Wright[4] in 1915 and Büssem and Eitel[5] determined its CaO-to-Al_2O_3 molar ratio to be 12:7 rather than 5:3. Since then, many investigations have been undertaken to determine the crystal structure and properties of $C_{12}A_7$.[6−9] The crystal lattice of $C_{12}A_7$ was found to belong to the space group of $I\bar{4}3d$, with a lattice constant of 1.199 nm and two chemical formula units per unit cell.[8] It has a specific nanoporous structure consisting of crystallographic nanocages with diameters of ∼0.4 nm (Figure 1, there are 12 cages per unit cell). Another unique feature of $C_{12}A_7$ is that it has

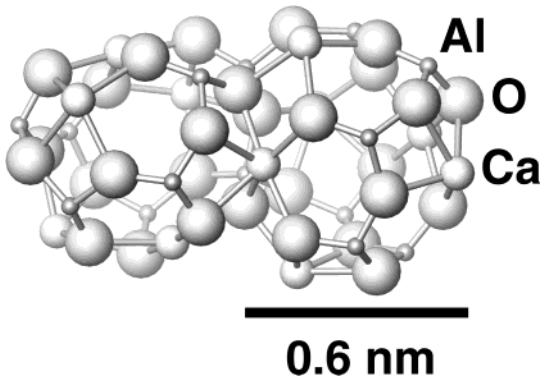

Figure 1. Structure of the framework of $C_{12}A_7$.

a positively charged lattice framework $[Ca_{24}Al_{28}O_{64}]^{4+}$, which is compensated for by anions accommodated within the nanocages. The property prevents $C_{12}A_7$ from forming in a very dry argon atmosphere,[7] and only poor yields can be achieved in dry nitrogen,[4,10] due to the lack of appropriate anions available in the atmosphere. Due to its porous structure and positively charged lattice framework, $C_{12}A_7$ is regarded as a counterpart of zeolite.

O^{2-} ions are usually present in the nanocages of $C_{12}A_7$ (two per unit cell), referred to as free oxygen or excess oxygen by cement chemists,[1,5−7] which are bound to Ca and are disordered over 12 cages in the unit cell. The free oxygen is easily replaced by other anionic species such as OH^-, F^-, or Cl^-, and the stability of substituted

* Corresponding authors. K. Domen: phone, +81-45-924 5238; fax, +81-45-924 5282; e-mail, kdomen@res.titech.ac.jp. H. Hosono: phone, +81-45-924 5359; fax, +81-45-924 5339; e-mail, hosono@msl.titech.ac.jp.
† Japan Science and Technology Corporation.
‡ Chemical Resources Laboratory, Tokyo Institute of Technology.
§ Materials and Structures Laboratory, Tokyo Institute of Technology.

(1) Nurse, R. W.; Welch, J. H.; Majumdar, A. J. *Trans. Br. Ceram. Soc.* **1965**, *64*, 323.
(2) Hallstedt, B. *J. Am. Ceram. Soc.* **1990**, *73*, 15.
(3) Chatterjee, A. K.; Zhmoidin G. I. *J. Mater. Sci.* **1972**, *7*, 93.
(4) Rankin, G. A.; Wright, F. E. *Am. J. Sci.* **1915**, *39*, 1.
(5) Büssem, W.; Eitel, A. *Z. Kristallogr.* **1936**, *95*, 175.
(6) Jeevaratnam, J.; Glasser, L. S. D.; Glasser, F. P. *Nature* **1962**, *194*, 764.
(7) Jeevaratnam, J.; Glasser, F. P.; Glasser, L. S. D. *J. Am. Ceram. Soc.* **1964**, *47*, 105.
(8) Bartl, H.; Scheller, T. *Neues Jahrb. Mineral. Monatsh.* **1970**, *35*, 547.
(9) Williams P. P. *Acta Crystallogr.* **1973**, *B29*, 1550.
(10) Aruja, E. *Acta Crystallogr.* **1957**, *10*, 337.

10.1021/cm034755r CCC: $27.50
Published on Web 11/26/2003

Table 1. Sample Preparation Conditions and Labels

sample	preparation/treatment conditions	S_{BET} (m^2/g)
$C_{12}A_7$-DryAir	sintering $CaCO_3$ and γ-Al_2O_3 under flowing dry air at 1350°C for 6h	1.5
$C_{12}A_7$-O_2	sintering $CaCO_3$ and γ-Al_2O_3 under flowing O_2 at 1350°C for 6h	1.3
$C_{12}A_7$-fp	fine powder obtained by jet-milling $C_{12}A_7{-}O_2$	13.9
A400	after TPD of $C_{12}A_7{-}O_2$, 400°C/O_2/1h	/
A500	after TPD of $C_{12}A_7{-}O_2$, 500°C/O_2/1h	/
A600	after TPD of $C_{12}A_7{-}O_2$, 600°C/O_2/1h	/
A700	after TPD of $C_{12}A_7{-}O_2$, 700°C/O_2/1h	/
A900	after TPD of $C_{12}A_7{-}O_2$, 900°C/O_2/1h	/

$C_{12}A_7$ decreases in the order $C_{12}A_7{-}F^- > C_{12}A_7{-}Cl^- > C_{12}A_7{-}OH^-$ (the designation F^-, Cl^-, and OH^- refer to the principal occluded species, but do not imply a precise stoichiometry).[7] Due to the presence of moisture in air, $C_{12}A_7$ prepared under ambient conditions is actually $C_{12}A_7{-}OH^-$. Upon heating or cooling in ambient atmosphere, water is adsorbed at temperatures lower than ~1050 °C, up to 1.3 wt % H_2O at 950 °C without significant change of the crystal structural parameters;[1,11,12] dehydration occurs at 1050 °C and above. Therefore, by controlling the atmosphere during preparation, $C_{12}A_7$ containing extremely high concentrations of active oxygen radicals O^- and O_2^-,[13,14] H^-,[15] or even electrons,[16] has recently been successfully synthesized. At room temperature, O^- and O_2^- are very stable against reaction with small amounts of moisture (for at least several months).[14]

Oxygen radicals (O^- and O_2^-) are highly reactive and play an important role in catalytic oxidation reactions.[17,18] Therefore, $C_{12}A_7$ containing large amounts of oxygen radicals has been investigated as a potential oxidation catalyst or O^- emitter. In fact, $C_{12}A_7$ has been used as a catalyst in the pyrolysis of *n*-hexane,[19] *n*-heptane,[20−22] and methylcyclohexane,[23] as well as in partial oxidation of methane to syngas.[24] However, the $C_{12}A_7$ samples used in these applications probably incorporates OH^-, as deduced from the preparation conditions.

The oxidation ability of $C_{12}A_7$ with high concentrations of oxygen radicals has been demonstrated to be high in preliminary experiments.[13] When oxygen radicals are available, Pt metal is oxidized to Pt oxide, whereas no reaction occurs without oxygen radicals. It has also been found that O^- can be emitted from $C_{12}A_7$ by applying an electric field, demonstrating its potential use as an O^- emitter.[25−28] However, the application of $C_{12}A_7$ in catalytic reactions or as O^- emitters involves the mobility and regeneration of the oxygen radicals, and this kind of important information remains unclarified in the literature. Furthermore, the formation mechanism of oxygen radicals remains little understood. In this work, the desorption behavior, formation mechanism, and regeneration ability of oxygen ion species in $C_{12}A_7$ were studied by electron-spin resonance (ESR), Raman spectroscopy, and temperature-programmed desorption (TPD) techniques, aiming to provide more information on possible applications.

2. Experimental Section

2.1. Sample Preparation. The preparation and treatment conditions of samples used in this study are listed in Table 1. Briefly, $C_{12}A_7$ samples were prepared by solid-state reaction of $CaCO_3$ and γ-Al_2O_3 powders with a molar ratio of 12:7 at 1350 °C for 6 h under either flowing dry air ($C_{12}A_7$-DryAir) or flowing O_2 ($C_{12}A_7{-}O_2$) at atmospheric pressure. X-ray diffraction (XRD) measurements indicated that pure $C_{12}A_7$ phase was formed in both samples. The as-prepared samples were then crushed by planetary milling to yield powders with BET surface areas of ca. 1.5 m^2/g. Jet-milling of $C_{12}A_7{-}O_2$ yielded a fine $C_{12}A_7$ powder ($C_{12}A_7$-fp) with a BET surface area of 13.9 m^2/g. The scanning electron microscopy (SEM) images in Figure 2 show that $C_{12}A_7{-}O_2$ is clearly more bulky than $C_{12}A_7$-fp. The average particle size of $C_{12}A_7{-}O_2$ was ca. 3 μm, while that of $C_{12}A_7$-fp was about 400 nm. Similar morphology was observed for $C_{12}A_7$-DryAir in comparison to $C_{12}A_7{-}O_2$.

2.2. Electron-Spin Resonance. ESR measurements were conducted at ~9.7 GHz (X-band) using a Bruker E580 spectrometer at 77 K. Spin concentrations were determined from the second integral of the spectrum using $CuSO_4{\cdot}5H_2O$ as a standard with an error of 10−20%. The ESR signal was decomposed by a Lorentzian function according to *g*-values of O_2^- ($g_{xx} = 2.002$, $g_{yy} = 2.008$, and $g_{zz} = 2.074$) and O^- ($g_{xx} = g_{yy} = 2.036$, and $g_{zz} = 1.994$).[17,18,29] A detailed description of ESR measurements of the oxygen species in $C_{12}A_7$ can be found elsewhere.[13,14]

2.3. Raman Spectroscopy. Raman spectra were measured at room temperature using two different Raman spectrometers, a JASCO NRS-2100 Raman spectrometer equipped with a liquid nitrogen cooled charge coupled device (CCD) detector (LN/CCD-1100PF, Princeton Instruments) and using the 514.5-nm line of an Ar^+ laser as the excitation source, and a Nicolet 960 Fourier transformation (FT) Raman spectrometer with a liquid nitrogen cooled Ge detector and using a YAG laser ($\lambda = 1064$ nm) as the excitation source. For most samples,

(11) Welch, J. H. (Reported by Nurse, R. W.) *Fourth Int. Symp. Chem. Cement, Nat. Bur. Stand. (US) Monograph No. 43* **1962**, *1*, 36.
(12) Roy, D. M.; Roy, R. *Fourth Int. Symp. Chem. Cement, Nat. Bur. Stand. (US) Monograph No. 43* **1962**, *1*, 307.
(13) Hayashi, K.; Hirano, M.; Matsuishi, S.; Hosono, H. *J. Am. Chem. Soc.* **2002**, *124*, 738.
(14) Hayashi, K.; Matsuishi, S.; Ueda, N.; Hirano, M.; Hosono, H. *Chem. Mater.* **2003**, *15*, 1851.
(15) Hayashi, K.; Matsuishi, S.; Kamiya, T.; Hirano, M.; Hosono, H. *Nature* **2002**, *419* 462.
(16) Matsuishi, S.; Toda, Y.; Miyakawa, M.; Hayashi, K.; Kamiya, T.; Hirano, M.; Tanaka, I.; Hosono, H. *Science* **2003**, *301*, 626.
(17) Lunsford, J. H. *Adv. Catal.* **1972**, *22* 265.
(18) Che, M.; Tench, A. J. *Adv. Catal.* **1983**, *32*, 1.
(19) Lemonidou, A. A.; Vasalos, I. A. *Appl. Catal.* **1989**, *54*, 119.
(20) Kumar, V. A.; Pant, K. K.; Kunzru, D. *Appl. Catal., A* **1997**, *162*, 193.
(21) Pant, K. K.; Kunzru, D. *Ind. Eng. Chem. Res.* **1997**, *36*, 2059.
(22) Pant, K. K.; Kunzru, D. *Chem. Eng. J.* **2002**, *87*, 219.
(23) Pant, K. K.; Kunzru, D. *Chem. Eng. J.* **1998**, *70*, 47.
(24) Goula, M. A.; Lemonidou, A. A.; Grünert, W.; Baerns, M. *Catal. Today* **1996**, *32*, 149.
(25) Li, Q.-X.; Hayashi, K.; Nishioka, M.; Kashiwagi, H.; Hirano, M.; Torimoto, Y.; Hosono, H.; Sadakata, M. *Appl. Phys. Lett.* **2002**, *80*, 4259.
(26) Li, Q.-X.; Hayashi, K.; Nishioka, M.; Kashiwagi, H.; Hirano, M.; Torimoto, Y.; Hosono, H.; Sadakata, M. *Jpn. J. Appl. Phys.* **2002**, *41*, L530.
(27) Hayashi, K.; Li, Q.-X.; Nishioka, M.; Matsuishi, S.; Torimoto, Y.; Hirano, M.; Sadakata, M.; Hosono, H. *Electrochem. Solid-State Lett.* **2002**, *5*, J13.
(28) Li, Q.-X.; Hosono, H.; Hirano, M.; Hayashi, K.; Nishioka, M.; Kashiwagi, H.; Torimoto, Y.; Sadakata, M. *Surf. Sci.* **2003**, *527*, 100.
(29) Soria, J.; Martínez-Arias, A.; Conesa, J. C.; Munuera, G.; González-Elipe, A. R. *Surf. Sci.* **1991**, *251/252*, 990.

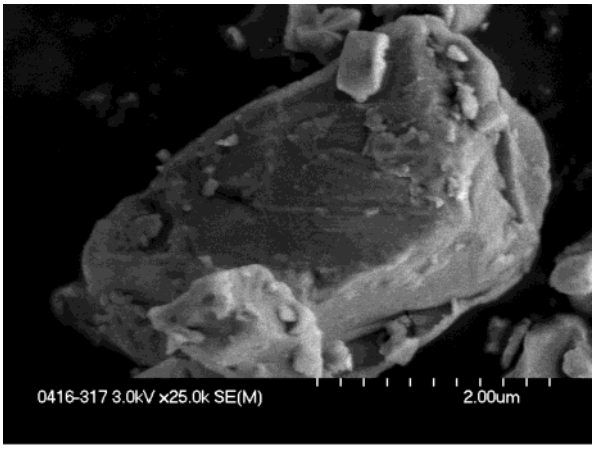

(a) C12A7-O_2

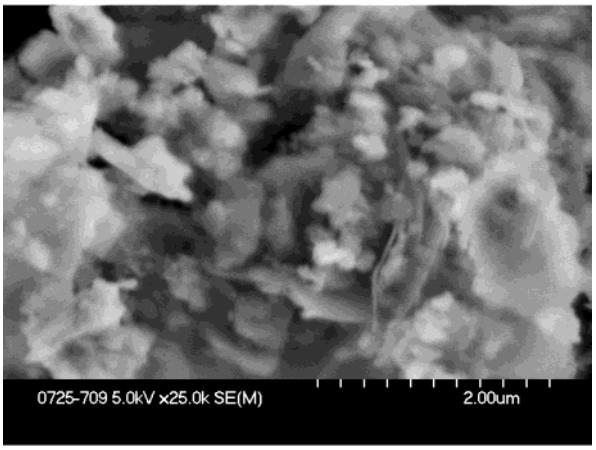

(b) C12A7-fp

Figure 2. SEM images of (a) $C_{12}A_7$-O_2 and (b) $C_{12}A_7$-fp.

good spectra were obtained using the YAG laser. However, a relatively clear spectrum for $C_{12}A_7$-DryAir could only be obtained by using the Ar^+ laser. No clear spectrum of $C_{12}A_7$-fp was obtained using either instrument due to the influence of strong fluorescence.

2.4. Temperature-Programmed Desorption. TPD experiments were performed on a Shimadzu TPD/TPSR system equipped with a mass spectrometer. Samples of 150 mg each were used for TPD runs. Unless otherwise indicated, samples were heated to 900 °C at 10 °C/min under 50-mL/min helium flow for TPD measurements. To further study the formation and desorption mechanisms of the oxygen species in $C_{12}A_7$, all the oxygen species in $C_{12}A_7$−O_2 were removed by TPD to 900 °C, and after being held at that temperature for 1 h, the sample was treated with O_2 at various temperatures for 1 h. Samples treated in this way are denoted in Table 1 by "A" plus the treatment temperature.

3. Results and Discussion

3.1. Oxygen Species in $C_{12}A_7$. ESR experiments were performed to investigate the existence of oxygen radicals in $C_{12}A_7$ samples. As shown in Figure 3, the ESR signal of $C_{12}A_7$-DryAir is sharp, whereas those of $C_{12}A_7$-O_2 and $C_{12}A_7$-fp are rather broad. All spectra can be decomposed into two components, attributable to O_2^- ($g_{xx} = 2.002$, $g_{yy} = 2.008$, and $g_{zz} = 2.074$) and O^- ($g_{xx} = g_{yy} = 2.036$, and $g_{zz} = 1.994$).[19,20,31] The concentrations

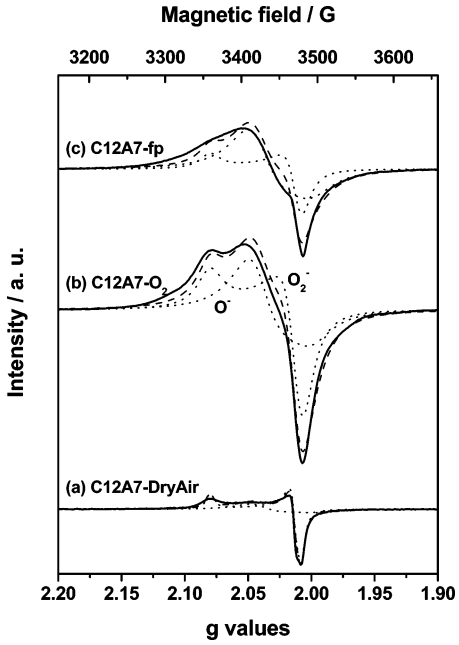

Figure 3. ESR spectra of (a) $C_{12}A_7$-DryAir, (b) $C_{12}A_7$-O_2, and (c) $C_{12}A_7$-fp.

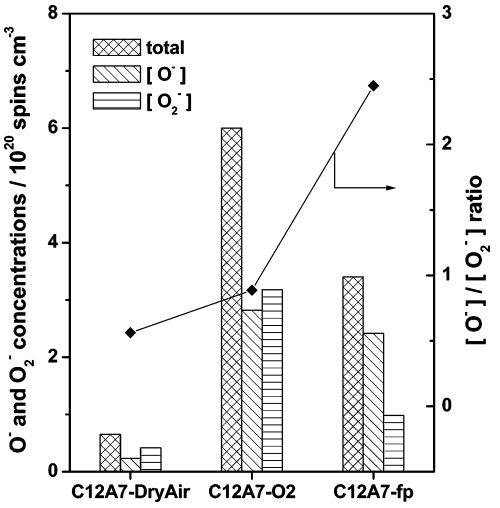

Figure 4. Concentrations of oxygen radicals (O^- and O_2^-) in different $C_{12}A_7$ samples.

of O^- and O_2^- are compared in Figure 4. For $C_{12}A_7$-DryAir, the concentrations of O^- and O_2^- are 2.3×10^{19} and 4.2×10^{19} cm^{-3}, respectively. When $C_{12}A_7$ was prepared in pure O_2 (101.3 kPa), the amounts of both O_2^- and O^- increased by about 10 times to the order of 10^{20} cm^{-3}. For $C_{12}A_7$-fp, the jet-milling process of $C_{12}A_7$-O_2 resulted in a reduction of the oxygen radical concentration, with more loss of O_2^- than of O^-.

The $[O^-]/[O_2^-]$ ratios for different $C_{12}A_7$ samples are also shown in Figure 4. A slight increase in the ratio is observed for $C_{12}A_7$ prepared at high O_2 partial pressure. The $[O^-]/[O_2^-]$ ratio is close to unity for $C_{12}A_7$-O_2, reflecting the formation mechanism of O^- and O_2^- radicals, as will be discussed later.

The presence of O_2^- in $C_{12}A_7$ was also confirmed by Raman spectroscopy using an Ar^+ laser (Figure 5). In

(30) Li, C.; Domen, K.; Maruya, K.; Onishi, T. *J. Am. Chem. Soc.* **1989**, *111*, 7683.

(31) Nakamoto, K. *Infrared and Raman spectra of inorganic and coordination compounds*, 5th ed.; John Wiley & Sons: New York, 1997; p 158.

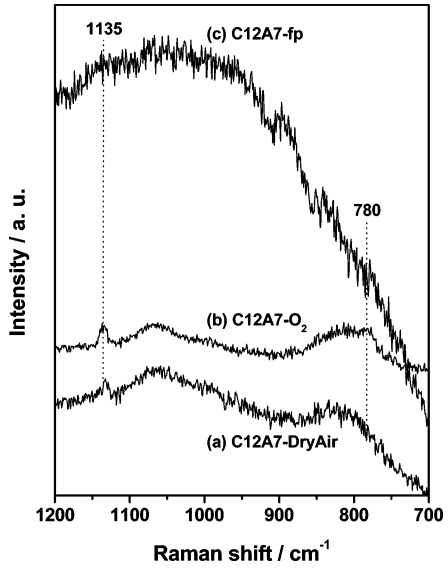

Figure 5. Raman spectra of (a) $C_{12}A_7$-DryAir, (b) $C_{12}A_7$-O_2, and (c) $C_{12}A_7$-fp (Ar^+ laser excitation source).

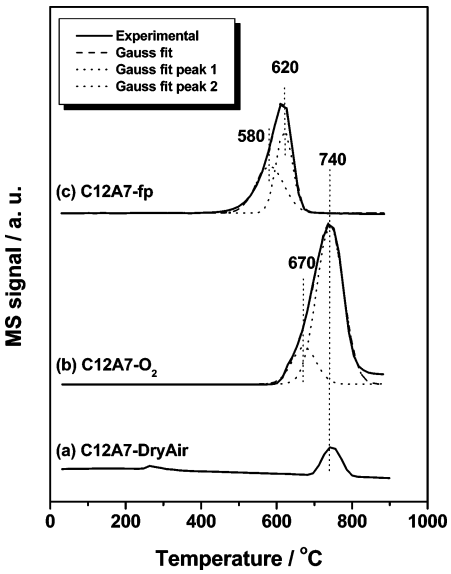

Figure 6. O_2-TPD profiles of as-prepared samples: (a) $C_{12}A_7$-DryAir, (b) $C_{12}A_7$-O_2, and (c) $C_{12}A_7$-fp. Heating rate: 10 K/min.

the Raman spectra of $C_{12}A_7$-DryAir and $C_{12}A_7$-O_2, one band at 1135 cm^{-1} can be clearly observed, attributed to the stretching vibration of O_2^-, the superoxide.[18,30] Interestingly, one weak band at 780 cm^{-1} can also be observed in the spectrum of $C_{12}A_7$-O_2 (Figure 5b). A Raman band appearing at ca. 780 cm^{-1}, sometimes with a shoulder, has been observed for a number of alkaline oxides and has been assigned to O_2^{2-}, the peroxide.[31] For $C_{12}A_7$-DryAir, the band at around 780 cm^{-1} is not well-resolved, and neither the 1135- nor the 780-cm^{-1} bands could be distinguished for $C_{12}A_7$-fp due to the influence of strong fluorescence.

3.2. Desorption Behavior of the Oxygen Species in $C_{12}A_7$. Figure 6 shows the TPD profiles of O_2 desorbed from the three as-prepared $C_{12}A_7$ samples. The total integrated intensities of the O_2 desorption peaks agree well with the ESR results given in Figure 4. For $C_{12}A_7$-DryAir, O_2 begins to desorb at around 700 °C, and maximum desorption occurs at ca. 740 °C. A much stronger desorption peak of O_2 is observed in the TPD

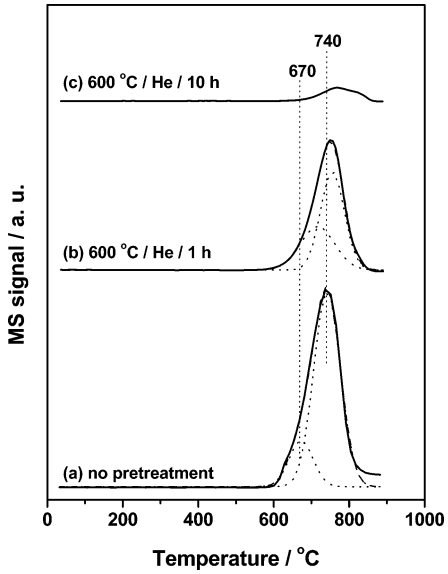

Figure 7. O_2-TPD profiles of $C_{12}A_7$-O_2 pretreated at different conditions before TPD: (a) no pretreatment, (b) treated under flowing helium at 600 °C for 1 h, and (c) treated under flowing helium at 600 °C for 10 h. Heating rate: 10 K/min.

profile of $C_{12}A_7$-O_2 (Figure 6b). The desorption starts at ca. 600 °C and attains a maximum at 740 °C. For $C_{12}A_7$-fp, desorption of oxygen species happens at a much lower temperature than that for $C_{12}A_7$-O_2 (about 120 °C lower at maximum desorption). Recalling that $C_{12}A_7$-O_2 is more bulky than $C_{12}A_7$-fp (Figure 2), it is deduced that the mobility of oxygen species in $C_{12}A_7$ is not high, and the desorption will be limited by mass transport in the bulk.

The apparently asymmetric desorption profiles of (b) and (c) in Figure 6 were each deconvolved into two components assuming a Gaussian line shape. $C_{12}A_7$-O_2 exhibited peaks at 670 and 740 °C, corresponding to the desorption of oxygen species from the outermost region of the C12A7 particle consisting surface layer and layers near the surface (hereafter referred to as the outermost region) and that from the bulk phase of $C_{12}A_7$, respectively. Peaks at 580 and 620 °C for $C_{12}A_7$-fp suggest that desorption of the oxygen species occurs more readily with decreasing particle size.

Figure 7 compares the TPD profiles of as-prepared $C_{12}A_7$-O_2 and $C_{12}A_7$-O_2 pretreated under flowing helium at 600 °C. Pretreatment for 1 h reduced the intensity of the O_2 desorption peak, without significant shift of the desorption temperature, while after 10 h of pretreatment, only a weak peak at ca. 760 °C remained, due to desorption of oxygen species from the bulk. These results further confirm the limited mobility of oxygen species in $C_{12}A_7$ and suggest that the diffusion of oxygen species from bulk to the outermost region requires more time and higher temperature than the simple release of oxygen species from the outermost region to the gas phase.

The influence of heating rate on desorption of the oxygen species is shown in Figure 8. Decreasing the heating rate has two consequences. First, the desorption peak temperature decreases with decreasing heating rate, which is a normal phenomenon for TPD experiments.[32,33] Second, after deconvolution of the profiles, it can be seen that the intensity ratio of the first peak

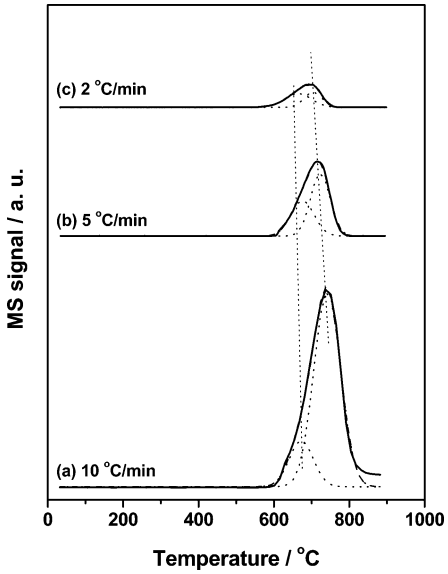

Figure 8. O_2-TPD profiles of $C_{12}A_7$-O_2 at various heating rates: (a) 10, (b) 5, and (c) 2 °C/min.

(*Peak 1*) to the second peak (*Peak 2*) increases with decreasing heating rate, further indicating that the two peaks originate from the desorption of oxygen species from the outermost region and bulk phase.

3.3. Regeneration of the Oxygen Species in $C_{12}A_7$. Regeneration of the oxygen species in $C_{12}A_7$ was evaluated by heating $C_{12}A_7$-O_2 under flowing helium at 900 °C for 1 h. A separate experiment confirmed that there was no oxygen desorption from the sample after this pretreatment process. This "oxygen-free" sample was then treated again in O_2 at various temperatures for 1 h. The concentrations of O^- and O_2^- for these regenerated samples were measured by ESR and they are plotted as a function of treatment temperature in Figure 9. The concentrations of O^- and O_2^- clearly increase with treatment temperature, suggesting that high temperature is crucial for the generation of these oxygen radicals. At 900 °C, the total concentration of oxygen radicals (O^- and O_2^-) was 1.4×10^{20} cm^{-3}, about one-fourth of that for $C_{12}A_7$-O_2.

The $[O^-]/[O_2^-]$ ratios of the regenerated samples are shown versus treatment temperature in Figure 9d. An increase in $[O^-]/[O_2^-]$ ratio is found upon elevating the treatment temperature, which indicates that O_2^- can be formed much more readily than O^- at relatively low temperature. The formation mechanism of O^- and O_2^- will be discussed in the next section.

Figure 10 shows the Raman spectra (YAG laser) for these regenerated samples and $C_{12}A_7$-O_2. All spectra were normalized by the band at 520 cm^{-1} associated with the vibration of the $C_{12}A_7$ lattice framework. The band at ~1135 cm^{-1} due to the existence of O_2^- is observed after the oxygen-free $C_{12}A_7$-O_2 is treated in O_2 at 600 °C and above, increasing in intensity with treatment temperature. The band at ~780 cm^{-1} attributable to O_2^{2-} can be seen more clearly than for $C_{12}A_7$-O_2 excited using an Ar^+ laser (Figure 5b), which unambiguously confirms the formation of peroxide species. Integrated intensities of the bands at ~1135 cm^{-1} (I_{1135}) and ~780 cm^{-1} (I_{780}) versus treatment temperature are plotted in Figure 11. Both I_{1135} and I_{780} increase with treatment temperature. At 400−700 °C, I_{780} increases, but only to a small extent. Currently, the amount of O_2^{2-} cannot be determined quantitatively due to the lack of coefficient factors for O_2^- and O_2^{2-} species.

TPD profiles of the regenerated samples are shown in Figure 12. When the $C_{12}A_7$ sample was heated in O_2 at 400 °C, only trace amounts of oxygen were desorbed. At higher temperatures, the desorption peak of O_2 becomes apparent. It is worth noting that the desorption peak from A600 (see Table 1 for denotation) is the strongest among the five regenerated samples. The desorption profiles can also be decomposed into two components: *Peak 1* (peak maximum at 670 °C) and *Peak 2* (at 740 °C), attributable to the desorption of oxygen species from the outermost region and from the bulk phase, respectively. The desorption of oxygen

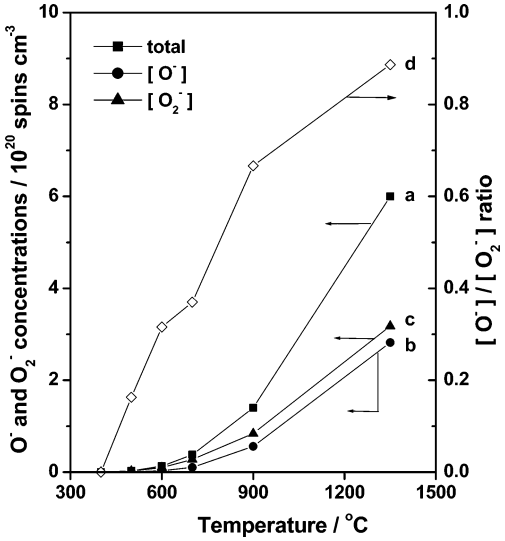

Figure 9. Concentrations of oxygen radicals (O^- and O_2^-) in $C_{12}A_7$-O_2 and $C_{12}A_7$-O_2 pretreated at various temperatures in oxygen: (a) total amount of O^- and O_2^-, (b) $[O^-]$, (c) $[O_2^-]$, and (d) $[O^-]/[O_2^-]$ ratio.

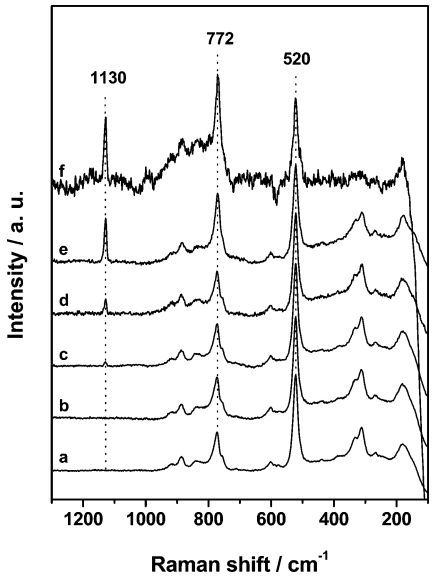

Figure 10. Raman spectra of (a) A400, (b) A500, (c) A600, (d) A700, (e) A900, and (f) $C_{12}A_7$-O_2 (heated at 1350 °C) (YAG laser excitation source).

(32) Falconer, J. L.; Schwarz, J. A. *Catal. Rev.−Sci. Eng.* **1983**, *25*, 141.
(33) Busser, G. W.; Hinrichsen, O.; Muhler, M. *Catal. Lett.* **2002**, *79*, 49.

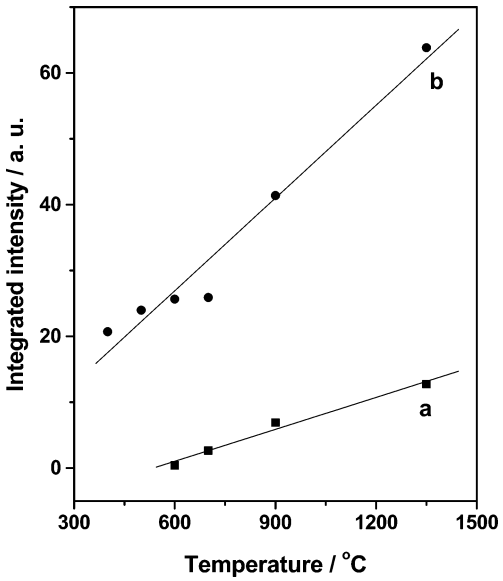

Figure 11. Integrated intensities of Raman bands at ~1135 cm^{-1} (I_{1135}, a) and ~780 cm^{-1} (I_{780}, b) in Figure 10 as a function of treatment temperature.

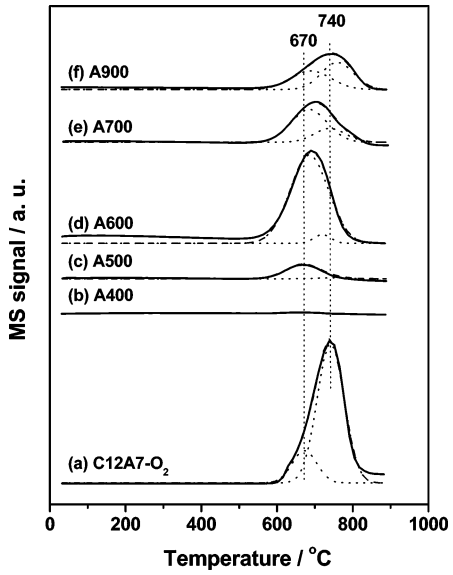

Figure 12. O_2-TPD profiles of (a) $C_{12}A_7$-O_2 (heated at 1350 °C), (b) A400, (c) A500, (d) A600, (e) A700, and (f) A900. Heating rate: 10 K/min.

species from the outermost region is clearly predominant for the samples treated at low temperatures (400−600 °C).

The integrated intensities of *Peak 1* and *Peak 2*, and the corresponding sum, are plotted in Figure 13 as functions of treatment temperature. Compared with Figure 9, it can be seen that the intensity of *Peak 2* (Figure 13b) increases in a manner similar to the total concentration of oxygen radicals (O^- and O_2^-) determined by ESR, in stark contrast to *Peak 1* (Figure 13a). Therefore, it is reasonable to assume that *Peak 2* originates from the desorption of oxygen radicals, whereas *Peak 1* is expected to be related to the desorption of other oxygen species.

As opposed to ESR and other spectroscopic techniques, TPD is unable to distinguish the nature of oxygen species on a solid, instead detecting the overall amount of desorbed O_2 which may originate from a

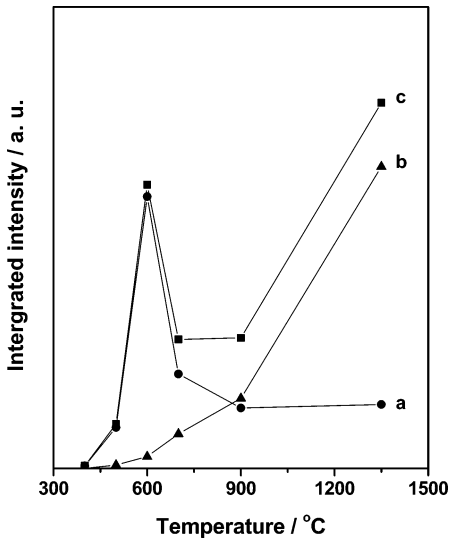

Figure 13. Quantitative results from the TPD profiles in Figure 9: (a) integrated intensity of the desorption peak at 670 °C (*Peak 1*), (b) integrated intensity of the desorption peak at 740 °C (*Peak 2*), and (c) sum of (a) and (b).

number of species.[32] From ESR and Raman results, it is clear that O^-, O_2^-, and O_2^{2-} species exist in $C_{12}A_7$ and as such the TPD profile must contain contributions from each. As the desorption of O^- and O_2^- contributes mainly to *Peak 2*, *Peak 1* can be considered to be entirely related to the desorption of O_2^{2-}. However, as shown in Figures 9 and 11, the amount of O^-, O_2^-, and O_2^{2-} increases with treatment temperature; therefore, if *Peak 1* is due to the desorption of O_2^{2-}, the O_2 desorption peaks from A700 and A900 must be stronger than A600. As the O_2 desorption peak A600 is the strongest among the five regenerated samples, *Peak 1* cannot be attributed entirely to the desorption of O_2^{2-}. As the free space within the $C_{12}A_7$ nanocages can accommodate molecular O_2, *Peak 1* is tentatively assigned to the desorption of encaged molecular oxygen. The presence of O_2 is critical for the formation of $C_{12}A_7$ crystalline phase and oxygen species,[13,34] and encaged molecular oxygen may serve as a precursor for the formation of various oxygen radicals. As shown in Figure 13a, a peak in the integrated intensity occurs at 600 °C, indicating that there is an energy barrier for the diffusion of gas-phase oxygen into the nanocages of $C_{12}A_7$. This step will be difficult at temperatures lower than 600 °C; yet above this temperature, encaged oxygen molecules readily react with other species to form various oxygen ion species, resulting in the loss of encaged O_2.

3.4. Mechanism of Oxygen Ion Species Formation. The existence of excess oxygen in $C_{12}A_7$ was first realized and quantified by Imlach et al.[34] The excess oxygen, presumed to be present in the form of peroxide ions or linkages, was determined to be 0.07−0.10 wt % and was detected by ordinary wet-chemical analysis. An oxygen-containing atmosphere or traces of moisture in inert atmospheres will serve as sources for this excess oxygen. The nature of this excess oxygen has already been investigated by ESR spectroscopy.[35,36] Hosono and

(34) Imlach, J. A.; Glasser, L. S. D.; Glasser, F. P. *Cem. Concr. Res.* **1971**, *1*, 57.
(35) Hosono, H.; Abe, Y. *Inorg. Chem.* **1987**, *26*, 1192.
(36) Stösser, R.; Nofz, M.; Gessner, W.; Schröter, C.; Kranz, G. *J. Solid State Chem.* **1989**, *81*, 152.

Abe[35] reported that the excess oxygen in $C_{12}A_7$ prepared by solid-state reaction appeared to be the superoxide radical ion O_2^-, present at concentrations up to ca. 4×10^{18} units/g. The occurrence of O_2^- is limited to $C_{12}A_7$ in the crystalline phases of the $CaO-Al_2O_3$ system. No ESR signal was detected for CaO, $3CaO{\cdot}Al_2O_3$ (C_3A), $CaO{\cdot}Al_2O_3$ (CA), $CaO{\cdot}2Al_2O_3$ (CA_2), and Al_2O_3, suggesting that the formation of O_2^- is related to the structural characteristics of $C_{12}A_7$. The O_2^- species can be replaced by an appropriate anion such as OH^-, F^-, and Cl^-, resulting in a decrease in O_2^- concentration and a slight modification of the lattice constant.[35] The present authors also observed that the ESR line shapes of O_2^- at temperatures near 77 K or higher appeared liquid-like, despite the host $C_{12}A_7$ being solid. This means that the O_2^- ions are encaged within the structural cavities, which enclose sufficient free space to contain the rapid tumbling motion of O_2^-.

For the first time, Hayashi et al.[13] recently found that, in addition to O_2^-, the O^- ion, which is the most active oxygen species, also exists in $C_{12}A_7$ prepared by sintering $CaCO_3$ and Al_2O_3 at 1350 °C in controlled atmospheres. High partial pressure of oxygen and low partial pressure of water favor the formation of oxygen radicals, particularly the most active O^-.[14] In $C_{12}A_7$-O_2, the concentrations of O^- and O_2^- are more or less equal (Figure 4), so the formation of O^- and O_2^- in pure O_2 may be explained by the following equations:

$$O_2\ (\text{atmosphere}) \rightarrow O_2\ (\text{cage}) \quad (1)$$

$$O^{2-}\ (\text{cage}) + O_2\ (\text{cage}) \rightarrow O^-\ (\text{cage}) + O_2^-\ (\text{cage}) \quad (2)$$

Because considerable amounts of molecular oxygen, O_2, are suggested to be present together with other oxygen ion species (Figures 12 and 13), it is deduced that the first step for the formation of oxygen ion species may involve the diffusion of oxygen molecules from the atmosphere into the cages (eq 1). Then the encaged O_2, O_2 (cage), reacts with free oxygen, O^{2-} (cage), to form O^- and O_2^-. For O_2^{2-}, it may be formed via the reaction of O_2 with free oxygen,

$$2O^{2-}\ (\text{cage}) + O_2\ (\text{cage}) \rightarrow 2O_2^{2-}\ (\text{cage}) \quad (3)$$

or via the combination of O^-:

$$2O^-\ (\text{cage}) \rightarrow O_2^{2-}\ (\text{cage}) \quad (4)$$

From the present results, it is clear that eqs 2 and 3 are favored at high temperature and high partial pressure of oxygen. For $C_{12}A_7$-DryAir prepared at lower O_2 pressure and the samples regenerated in O_2 at low temperatures, more O_2^- is formed than O^- (Figures 4 and 9). This implies the ready combination of O^- ions to form O_2^{2-} (eq 4) under these conditions.

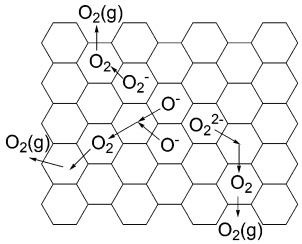

Figure 14. Proposed model for desorption of oxygen radicals (O^-, O_2^-, O_2^{2-}) in $C_{12}A_7$.

The mechanism of oxygen ion species formation can therefore be summarized into the following steps. First, O_2 molecules in the gas phase diffuse into the nanocages of $C_{12}A_7$ in the outermost region. Second, the encaged molecular oxygen reacts with anionic species in $C_{12}A_7$ to form oxygen ion species, and finally, these oxygen species diffuse inside the nanocages of $C_{12}A_7$.

3.5. Mechanism of Oxygen Species Desorption. The desorption of oxygen species is expected to occur in a reverse manner to the formation process. From the present TPD results, the desorption of oxygen species in $C_{12}A_7$ may proceed in three steps: (1) diffusion of oxygen species from bulk to the outermost region, (2) decomposition of oxygen species into oxygen molecules, and (3) release of molecular oxygen into the gas phase. The diffusion of oxygen species or oxygen molecules from bulk to the outermost region is considered to be the rate-limiting step. A simple model, as shown in Figure 14, is proposed to describe the desorption of these oxygen species, where the hexagons represent the nanocages of $C_{12}A_7$.

4. Conclusions

Various oxygen ion species, including O^-, O_2^-, and O_2^{2-}, were observed to exist in $C_{12}A_7$ at high concentrations ($\sim 10^{20}$ cm^{-3}). These oxygen species in $C_{12}A_7$ become mobile and desorb at 600 °C and can be regenerated by heating in O_2 at temperatures higher than 400 °C. The formation of oxygen species is proposed to involve the diffusion of O_2 molecules from the atmosphere into nanocages of $C_{12}A_7$ followed by reactions of this entrapped oxygen with O^{2-} ions. The desorption of these species occurs in a reversal of this process and is controlled by mass transport via small open windows of the nanocages of $C_{12}A_7$. The present results draw a clear picture of the formation, desorption, and regeneration of the active oxygen species in $C_{12}A_7$ and can be expected to be useful in the application of this unique material as an O^- emitter, as well as to specific chemical and electrochemical reactions.

CM034755R